The Astrophysical Journal, 842:12 (7pp), 2017 June 10 https://doi.org/10.3847/1538-4357/aa7386

Neon-like Iron Ion Lines Measured in NIFS/Large Helical Device (LHD) and *Hinode*/EUV Imaging Spectrometer (EIS)

Tetsuya Watanabe[1,2], Hirohisa Hara[1,2], Izumi Murakami[2,3], Daiji Kato[2,3], Hiroyuki A. Sakaue[3], Shigeru Morita[2,3], Chihiro Suzuki[3], Naoki Tamura[3], Norimasa Yamamoto[4], and Nobuyuki Nakamura[5]
[1] National Astronomical Observatory, National Institutes of Natural Sciences 2-21-1 Osawa Mitaka Tokyo, 181-8588, Japan; watanabe@uvlab.mtk.nao.ac.jp
[2] SOKENDAI [Graduate University for Advanced Studies] Hayama, Miura-gun, Kanagawa, 240-0193, Japan
[3] National Institute for Fusion Science, National Institutes of Natural Sciences 322-6 Oroshi-cho, Toki Gifu, 509-5292, Japan
[4] Chubu University 1200 Matsumoto-cho, Kasugai Aichi, 487-0027, Japan
[5] The University of Electro-Communications 1-5-1 Chofugaoka, Chofu Tokyo, 182-8585, Japan
Received 2016 December 26; revised 2017 May 11; accepted 2017 May 14; published 2017 June 7

Abstract

Line intensities emerging from the Ne-sequence iron ion (Fe XVII) are measured in the laboratory, by the Large Helical Device at the National Institute for Fusion Science, and in the solar corona by the EUV Imaging Spectrometer (EIS) on board the *Hinode* mission. The intensity ratios of Fe XVII λ 204.6/λ 254.8 are derived in the laboratory by unblending the contributions of the Fe XIII and XII line intensities. They are consistent with theoretical predictions and solar observations, the latter of which endorses the in-flight radiometric calibrations of the EIS instrument. The still remaining temperature-dependent behavior of the line ratio suggests the contamination of lower-temperature iron lines that are blended with the λ 204.6 line.

Key words: atomic data – line: formation – plasmas – Sun: corona – Sun: UV radiation

1. Introduction

The Sun is sometimes considered as "a laboratory in space" that shows very interesting phenomena taking place on a gigantic scale, and spectroscopic observation of extreme ultraviolet (EUV) emission lines provides unique information about the physical conditions in the outer atmosphere of the Sun. The *Hinode* mission has been observing the Sun for a decade in orbit, and is providing opportunities for better understanding the dynamic and violent nature of solar coronal plasmas through high-resolution EUV spectroscopic observations conducted with the EUV Imaging Spectrometer (EIS) on board (Culhane et al. 2007), and emission lines have been intensively observed that are emerging from the abundant iron element at various ionization stages in the solar atmosphere. Highly charged iron plasmas are also created in the Large Helical Device (LHD), which is set up at the National Institute for Fusion Science (NIFS), by injecting a TESPEL (tracer-encapsulated-pellet; Sudo et al. 2002; Sudo & Tamura 2012) or an impurity pellet (Huang et al. 2014a). Modeling of iron ions is tested and improved with both solar and laboratory measurements. The analysis tool has been developed to handle plasmas in non-equilibrium states, and this "time-dependent collisional-radiative (CR)" model is applied as a common tool to both solar and laboratory plasmas (Yamamoto et al. 2008; Watanabe et al. 2009, 2013; Murakami et al. 2014). This model tried to use improved atomic data sets by evaluating theoretical calculations and the measurements in the laboratory.

Ne-sequence iron ions, Fe XVII, are formed around the temperature of log $T_e \sim 6.7$, which almost corresponds to the maximum temperature reached in solar active regions. Based on their nanoflare models, Patsourakos & Klimchuk (2006) predicted the line profiles for Fe XVII (254.8 Å) observed by EIS. The intensity ratio of this line to that of 204.6 Å is solely determined by the branching ratio of the common upper level ($2p^5 3p\,^1S_0$). The EIS instrument on board the *Hinode* mission has detected several weak Fe XVII emission lines appearing in its observing wavelengths (170–210 Å and 250–290 Å), and they are identified as those from the transitions between $2p^5$ 3s/3p–$2p^5$ 3p/3d. The observed line intensity ratios are compared among them with our theoretical calculations. We found that many of them are blended by lower-temperature weak coronal lines, and that the photon branching ratio of the $2p^5$ 3p $^3S_0$ level to the $2p^5$ 3s levels is incorrect by about a factor of 2. Warren et al. (2008) analyzed the Fe XVII line spectra in a B2-class flare (2007 June 2), which were identified by Del Zanna & Ishikawa (2009). Table 1 of their paper summarized the Fe XVII line intensities during the flare compared with theoretical line ratios derived from the CHIANTI code. They found a systematic deviation from the theoretical values, and the Fe XVII λ 204.6/ λ 254.8 line ratio exceeded more than a factor of 2, different from the theoretical prediction of 1.1. In the analysis of the same flare, Del Zanna (2008) also found a discrepancy: Fe XVII λ254.8 is 50% weaker than the theoretical prediction. These results initiated a revisit of the radiometric calibration of the EIS instrument, and the authors finally concluded that the sensitivity degradation in the EIS short-wavelength channel showed significantly longer decay times than the long-wavelength channel (Del Zanna 2013; Warren et al. 2014).

The LHD in the NIFS is used to validate the CR models and the atomic data used for iron ions. The LHD can maintain stable plasmas even after impurity elements are injected by an impurity pellet (Huang et al. 2014a) or a TESPEL (Sudo et al. 2002; Sudo & Tamura 2012). The LHD has various diagnostic systems for measuring electron temperature, density, and other plasma properties. It is found that we can produce plasmas in the LHD with electron temperatures similar to those in the solar corona. We can therefore use TESPELs and/or impurity pellets to inject iron into LHD plasmas and measure EUV spectra to compare them with the model calculations (Yamamoto et al. 2008; Murakami et al. 2010; Sakaue et al. 2011). The CR model for Fe XIII evaluated using the LHD experiments has been applied to analyze solar spectra measured by *Hinode* EIS

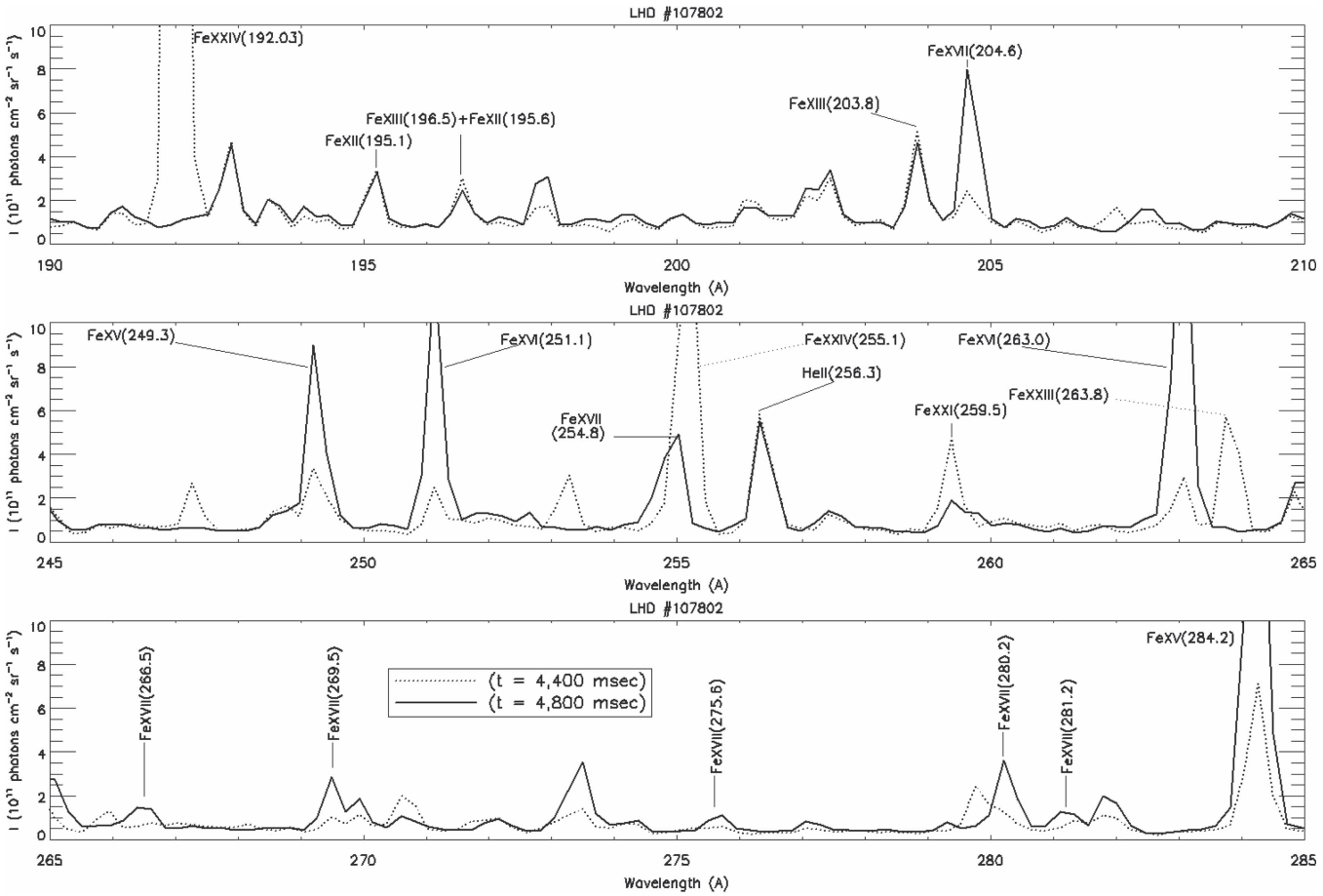

Figure 1. LHD spectra taken at the LHD shot number of 107,802.

to estimate the electron density distribution in a solar active region (Watanabe et al. 2009).

We compare in this paper the intensity ratios of the Fe XVII lines measured in the LHD in the NIFS with the solar observations and the model predictions.

2. Laboratory Measurements and Solar Observations

2.1. Laboratory Measurements

Highly charged iron ions are generated by injecting iron TESPELs into the LHD at the NIFS in Toki City in Japan. Discharges in these shots last several seconds, and temperatures reach 2–3 keV (~20–30 MK) during the main phase of discharge. However, the temperatures are then intentionally reduced to "solar coronal" temperatures by injecting TESPELs that are doped with iron powder and by reducing the power of the neutral beams and changing their injection directions. Figure 1 shows that iron line emissions at various ionization stages (Fe VIII to Fe XXII) start to emerge more prominently, while emission lines from Fe XXIV dominate in the spectral region near 200 Å and 255 Å during the main discharge phase before the injection of the TESPEL.

EUV spectra in the wavelengths of 100–300 Å are taken by a flat-field EUV spectrometer with a varied-line-spacing groove grating (1200 grooves mm^{-1} at the grating center) (Chowdhuri et al. 2007) developed to study emission spectra from medium-Z impurities in LHD (Zhang et al. 2015). The spectrometer covers the wavelength range of 50–500 Å using a laminar-type holographic grating, which is superior in suppressing the higher-order light, and in uniformity of sensitivity in the full wavelength range. A spectral resolution of ~0.24 Å at 200 Å is successfully achieved on the CCD detector (0.198 Å/channel). A stack of aluminum foil is placed in front of the grating in order to reduce the emissions emerging at wavelengths shorter than 170 Å. This is necessary to avoid spectral contamination from higher energy iron lines that may appear in the second-, third-, or fourth-order spectral ranges. A new technique for the absolute calibration is introduced by comparing the EUV bremsstrahlung profile with the visible bremsstrahlung profile, whose absolute value has previously been calibrated using a standard lamp (Dong et al. 2011).

We analyzed the spectra measured for the plasma in the shot number of 107,802 obtained in the LHD experiment (Murakami et al. 2014). Three tangential neutral beams (NBIs) are injected during $t = 3.3$–4.3 s after the start of discharge, and two perpendicular NBIs are injected at $t = 4.2$–6.2 s. The central elecron temperature started to decrease drastically at $t = 4.3$ s, reached its minimum at $t = 5$ s, and then increased again (see Figure 2(a)).

Iron lines at various ionization stages are identified in the spectra, including the seven Fe XVII lines listed in the Table 1 of Murakami et al. (2014), as well as 3s–2p and 3d–2p transitions emitted in the wavelength range of 15–17 Å (Huang et al. 2014b). Figure 2(b) shows the temporal evolution of the blended iron line intensities appearing at the wavelengths of 195.1 Å, 196.6 Å, 203.8 Å, 204.6 Å, and 254.8 Å, where the line profiles are fitted with a single-Gaussian shape. The wavelength scale is calibrated with prominent Fe XXIV lines

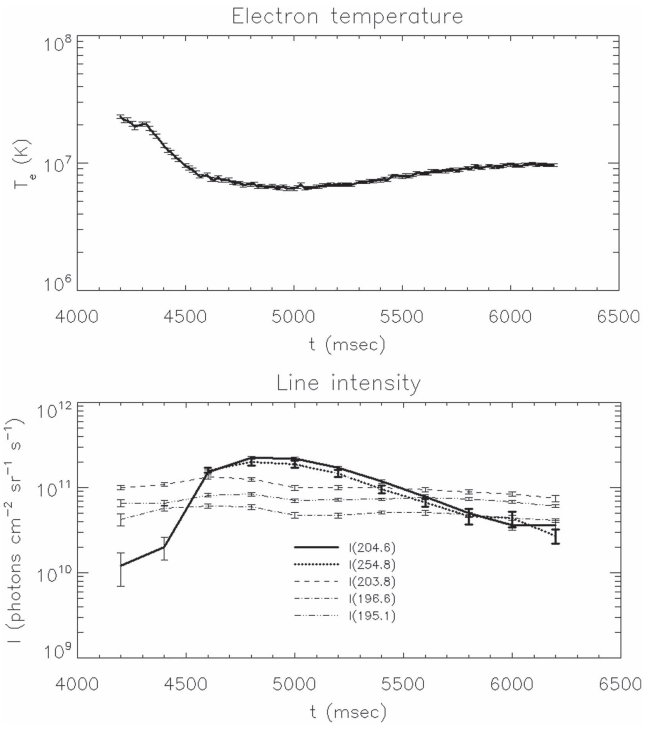

Figure 2. (a) Electron temperature (T_e) at the geometrical center at the shot 107,802 discharge. A few times, the NBI controls take place after $t = 3.3$ s. (b) Temporal evolution of the iron line blend intensities at 195.1 Å, 196.6 Å, 203.8 Å, 204.6 Å, and 254.8 Å. Error bars indicate the ranges of the photon statistical noise in the two panels.

and other impurity lines. The line feature at 254.8 Å is embedded in the strong Fe XXIV line at 255.1 Å and cannot be measured before $t = 4.6$ s. The temporal behaviors of the other Fe XVII lines are similar to those of the lines at 204.6 Å and 254.8 Å. See Figure 4 of Murakami et al. (2014) for more details.

2.2. Collisional-radiative Models

Murakami et al. (2014) have constructed a CR model with the quasi-steady-state approximation to calculate the population densities of excited states for an iron ion. The population densities of excited states are assumed to relax fast enough to equilibrium states when they are compared to the timescales for changes in plasma properties and ion densities, and the rate equations for population densities are solved as in steady state. Excited states up to the principal quantum number $n = 5$ are considered, and a total of 157 fine-structure levels are included. Processes of radiative decay, electron-impact excitation and de-excitation, electron-impact ionization, and proton-impact excitation and de-excitation are also included. Recombination processes are not included in this model because LHD plasmas are mostly in an ionizing plasma phase, and in such cases, recombination processes are not important for the spectral analysis. Energy levels, transition probabilities, and electron-impact excitation and ionization cross-sections are calculated with the HULLAC atomic code developed by Bar-Shalom et al. (2001). Proton-impact rate coefficients are taken from recommended data (Skobelev et al. 2010). The Fe XVII line intensity ratios obtained from this model are consistent with those obtained from the CHIANTI atomic data base (Dere et al. 1997). Version 8 of the code (Del Zanna et al. 2015) in the CHIANTI data base is basically applied for the data analysis obtained from LHD and *Hinode*/EIS. For Fe XII and Fe XIII lines, the CHIANTI code in version 6 (Dere et al. 2009) also generates very consistent values for their line ratios to those of solar corona and laboratory experiments (Yamamoto et al. 2008; Watanabe et al. 2009). The ADAS package (Summers 2004) contains various atomic data sets for iron ions, and we use the data set of "lgy09" (Liang & Badnell 2010) for comparison, in which the effective excitation collision strengths are obtained by the ICFT R-matrix method with 209 levels.

2.3. Solar Observations

Long-exposure full CCD spectra taken during the "first light" period of the EIS instrument (Watanabe et al. 2007; Brown et al. 2008) are used to analyze the Fe XVII line. The full CCD observation with six diffrent exposure times was performed from 2006 November 4 23:40:44. In this observation, slit spectra are taken with the EIS long slit (1 arcsec width and 512 arcsec height), and covered both the quiet Sun (QS) and an active region (NOAA AR 10921) along the solar-Y (N–S) direction. The slit location is indicated in the slot image of Fe XV taken during the following observation, which started on 2006 November 5 00:55:30. See Figure 1 of Watanabe et al. (2007). The laminar concave grating of the EIS spectrograph has a groove density of 4200 grooves mm^{-1} and a spectral dispersion of $\sim$0.023 Å/pixel (Culhane et al. 2007). Line intensities can be obtained from the pre-launch calibration (Lang et al. 2006), but the in-flight radiometric calibration of the EIS suggests that the long-wavelength (LW) channel might suffer from a significant degradation with time, while in the short-wavelength (SW) channel, the longer wavelengths do not show such significant degradations and the shorter wavelengths show some degradation (Del Zanna 2013). This effect is discussed in the following sections.

Figure 3 shows the scatter plots of the Fe XVII line intensities to those of Fe XVII λ 254.8 line. Line intensities in unit of ergs cm^{-2} s^{-1} sr^{-1} are plotted in Figure 3 by adopting the in-flight calibration from the paper of Del Zanna (2013), in which the parameters for the polynomial fit are given in the Appendix B. Filled circles show the data obtained from the active region (AR) cores, where the pixel numbers along the slit counted from the solar south are 261–290, and open circles are those from the AR southern peripheral region, where the pixel numbers are 241–260. The correspondence of the pixel numbers along the slit direction to the Y coordinates is found in Figure 7 of Watanabe et al. (2007). The broken line in each panel in Figure 3 indicates the linear regression line derived by the least-squares method. The top left panel in Figure 3 shows that the λ 204.6 line becomes relatively stronger in the AR peripheral regions, namely in the region that is cooler than the AR core, which suggests that the Fe XVII at 204.6 Å is blended with the lower coronal temperature lines (Del Zanna & Ishikawa 2009).

3. Data Analysis

3.1. Unblending Procedure of Fe XII/XIII Lines in LHD Spectra

The Fe XVII line features identified in the LHD spectra are considered to be blended with the Fe XII and Fe XIII lines that originate from the cooler peripheral region of the LHD

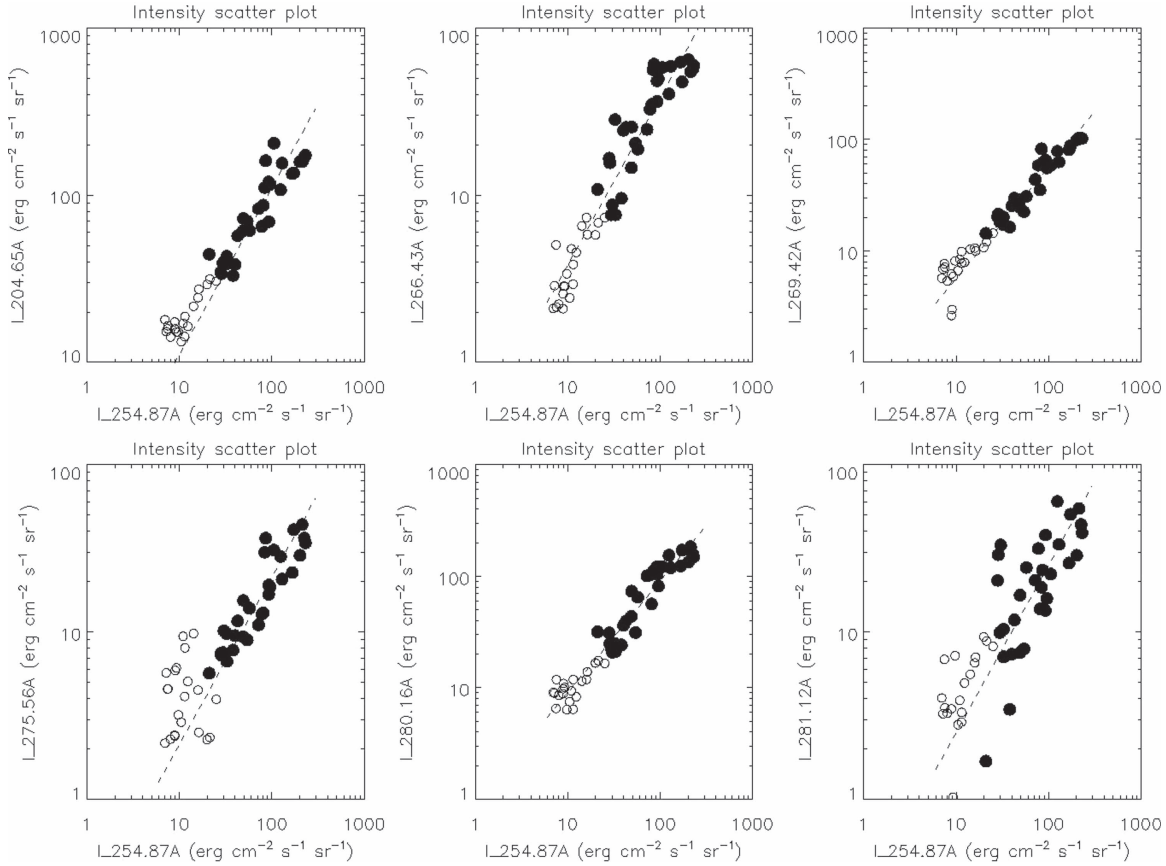

Figure 3. Scatter plots of the Fe XVII line intensities against Fe XVII λ 254.8. Filled circles show the data obtained from the active region cores (pixels 261–290 along the slit aligned in the solar N–S direction), and open circles are for the AR peripheral region (pixels 241–260) adjacent to the core region.

plasmas, where the electron temperatures decreases to the Fe XIII/XII forming temperatures. See Figure 2 of Murakami et al. (2014), which shows the radial temperature distribution of the created LHD plasma measured by Thomson scattering. The sight line of the EUV spectrometer extends from the low-temperature peripheral region to the high-temperature central region of the LHD plasma. Referring to the EIS spectra with the better spectral resolution, we assume the following in the course of our analysis: (a) the emission line feature at 195.1 Å is purely from the Fe XII lines at the same wavelengths, (b) the line complex around 196.6 Å consists of Fe XIII 196.5 Å and Fe XII 196.6 Å, (c) the line complex around 203.8 Å consists of Fe XII 203.7 Å and Fe XIII 203.8 Å, and (d) the feature at 204.6 Å consists of Fe XVII 204.6 Å and Fe XIII 204.3 Å + 204.9 Å. All of these Fe XII and Fe XIII lines are density sensitive. Therefore, after we derive electron density in the low-temperature peripheral region of LHD plasmas, we estimate the blended Fe XIII intensities at 204.3 Å and 204.9 Å, and try to reduce the intensity of the Fe XVII line at 204.6 Å.

In order to test the accuracy of this procedure for the n_e estimation in the LHD spectra with the lower spectral resolution, we first generate a set of line complex intensity distributions along the slit direction from the same EIS spectra as were used in Section 2.3 (Figure 4(a)) to simulate the line blending in the LHD spectra. The Fe XII electron densities can be estimated simply from the intensity ratios of λ 186.8/λ 195.1 (dotted curve in Figure 4(b)). The electron densities from

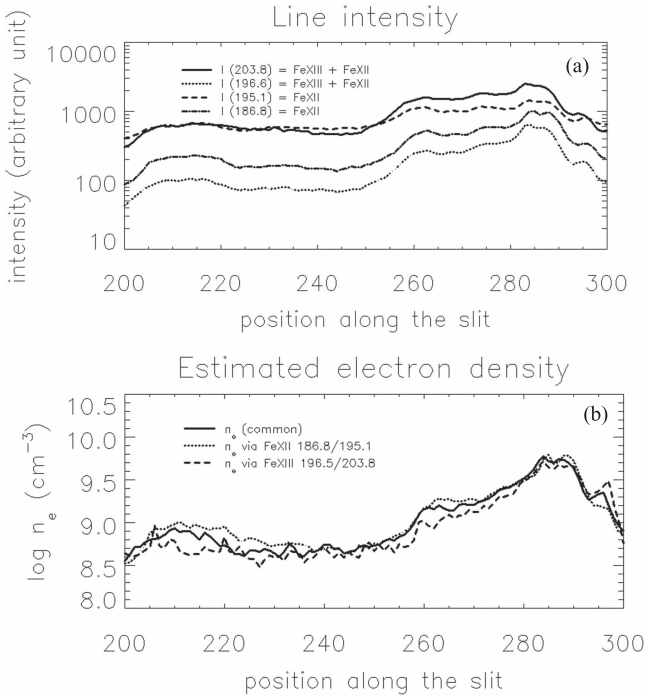

Figure 4. (a) Summed intensities of the nearby Fe XII and Fe XIII lines in wavelength. The abscissa is the pixel number along the slit. (b) Estimated electron densities (a) assuming common among Fe XII and XIII ions (solid), (b) by Fe XII density-sensitive line pairs (dotted), and (c) by Fe XIII line pairs (dashed).

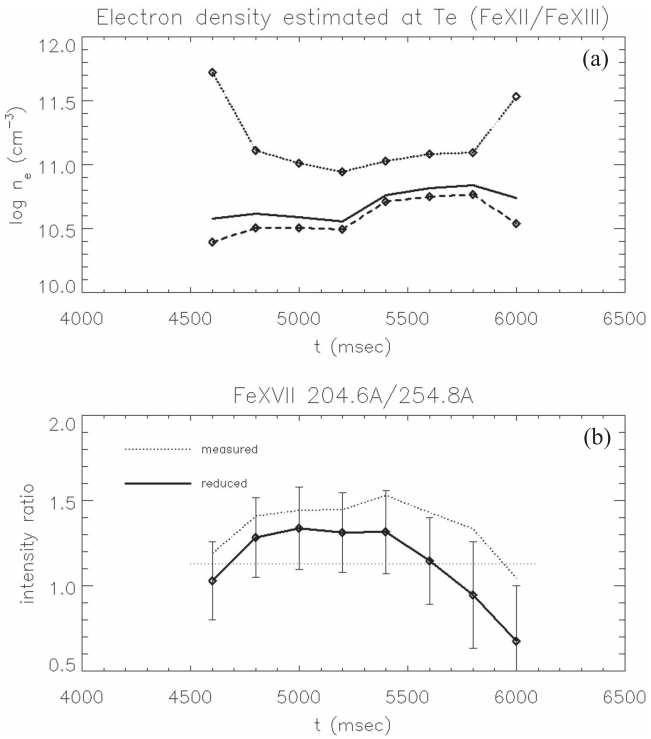

Figure 5. (a) Electron densities for the LHD plasma plottted against time since the discharge of shot 107,802. The line types are the same as in Figure 4(b). (b) Reduced Fe XVII line ratios by unblending the contributions of the Fe XII and XIII lines. The horizontal thin dotted line indicates the line intensity ratio averaged at the eight epochs in discharge 107,802. Error bars show photon noise ranges only.

the Fe XIII line ratios are then derived from the reduced intensity ratios of λ 196.6/λ 203.8 by subtracting the contribution of the Fe XII line at 203.7 Å from the denominator and the contribution of the Fe XII line at 196.6 Å from the numerator with the help of the theoretical model, CHIANTI version 8 in this case (dashed curve). If we assume common electron densities for the Fe XII/XIII line emitting plasmas, we may be able to obtain them from the intensity ratios of λ 196.6/λ 203.8 by comparing them with the theoretical predictions (solid curve). Electron densities derived from the procedure described above are basically consistent with those obtained from the EIS spectra of the original spectral resolution (see Figure 7 of Watanabe et al. 2007). The discrepancies in estimated log n_e from Fe XII and Fe XIII are much reduced in version 8 and give slightly lower values (~0.3 dex) than those derived from version 6, although the values estimated from the Fe XII line ratios are still somewhat higher than those derived from the Fe XIII line ratios, mainly reflecting physical differences of the emitting regions the two plasmas (Young et al. 2009).

3.2. Reduced Fe XVII Line Intensity at 204.6 Å in LHD Spectra

After we confirmed that we were able to estimate the contribution of the blended line intensities of Fe XIII and Fe XII in the analysis of EIS spectra, we applied the same method to the Fe XVII line complex around λ 204.6 Å in the LHD spectra to unblend the Fe XIII and XII line intensities.

The results are summarized in Figure 5. The time evolution of the electron density for low-temperature LHD peripheral plasmas is plotted in Figure 5(a), where the electron density (n_e) is estimated to be log n_e (cm^{-3}) ~ 10.5–11.8 after the NBI controls, slightly higher in the later phases of discharge. The estimated electron densities are somewhat lower than those measured by Thomson scattering at t = 4.3 s and t = 4.9 s (see Figure 2 of Murakami et al. 2014), but these line intensity ratios of Fe XII and XIII are located in the range that is close to the high-density limit, and the apparent large difference in the absolute n_e values derived from Fe XII and Fe XIII does not affect the estimation of the blended Fe XIII/XII line intensities much, and therefore is negligible in the following analysis results.

We take this contribution of the Fe XIII emissions to the emission line intensity at 204.6 Å into account and plot the Fe XVII λ 204.6/λ 254.8 ratios against time after the start of discharge in Figure 5(b). No lines are assumed to be blended in the Fe XVII λ 254.8 line, and a common electron density is assumed for the Fe XII/XIII emitting plasmas. The measured ratio is reduced to 20%–30% as a result of subtracting the Fe XIII line contribution, and the average value (~1.12) is very close to the theoretically predicted constant vlaue of ~1.1, although the temporal variation, henceforth, the temperature dependence of the line ratios, could not be completely eliminated in this analysis. The average value at the four epochs (t = 4.8–5.4 s) is rather close to ~1.3, when the line complexes at 204.6 Å are the strongest and the electron temperatures are the lowest during the discharge.

4. Discussion and Summary

The Fe XVII line intensity ratios obtained from the solar active region in Section 2.3 and the LHD experiment are plotted against electron temperature in Figure 6, in which the revised sensitivity proposed by Del Zanna (2013) is adopted for the EIS radiometric calibration. The LHD experimental results clearly show that the Fe XVII line branching ratio of λ 204.6/λ 254.8 is close to the theoretical value of ~1.1, which means that the revised in-orbit EIS sensitivity calibration (Del Zanna 2013; Warren et al. 2014) makes the solar data consistent with the laboratory data. The apparent temperature dependence of the line ratio can be attributed to a scenario in which the Fe XVII λ 204.6 line is blended by the weak iron emission line at its lower ionization stages (Del Zanna & Ishikawa 2009).

The line intensity ratios except for the ratio of λ 204.6/λ 254.8 do not suffer from a large degradation of the pre-flight sensitivity in the EIS-LW band, and they are almost consistent with the data obtained from the SKYLAB experiment (Doschek et al. 1991). All of the Fe XVII lines apearing in the EIS-LW band are very weak, however, and they show systematically higher line ratios relative to the apparently single line at λ 254.8. This means that these weak lines can be blended with other weaker lines, or it may indicate that the intensity of the λ 254.8 line is somewhat weaker than its theoretical predictions. The former is especially the case for the λ 269.4 line, as it could be blended with an Fe XIV line (Murakami et al. 2014).

Figure 6 shows that our CR model is marginally consistent with the LHD measurements and the EIS and other solar observations for the FeXVII line ratios. Murakami et al. (2014) discussed that the CHIANTI version 8 and the ADAS

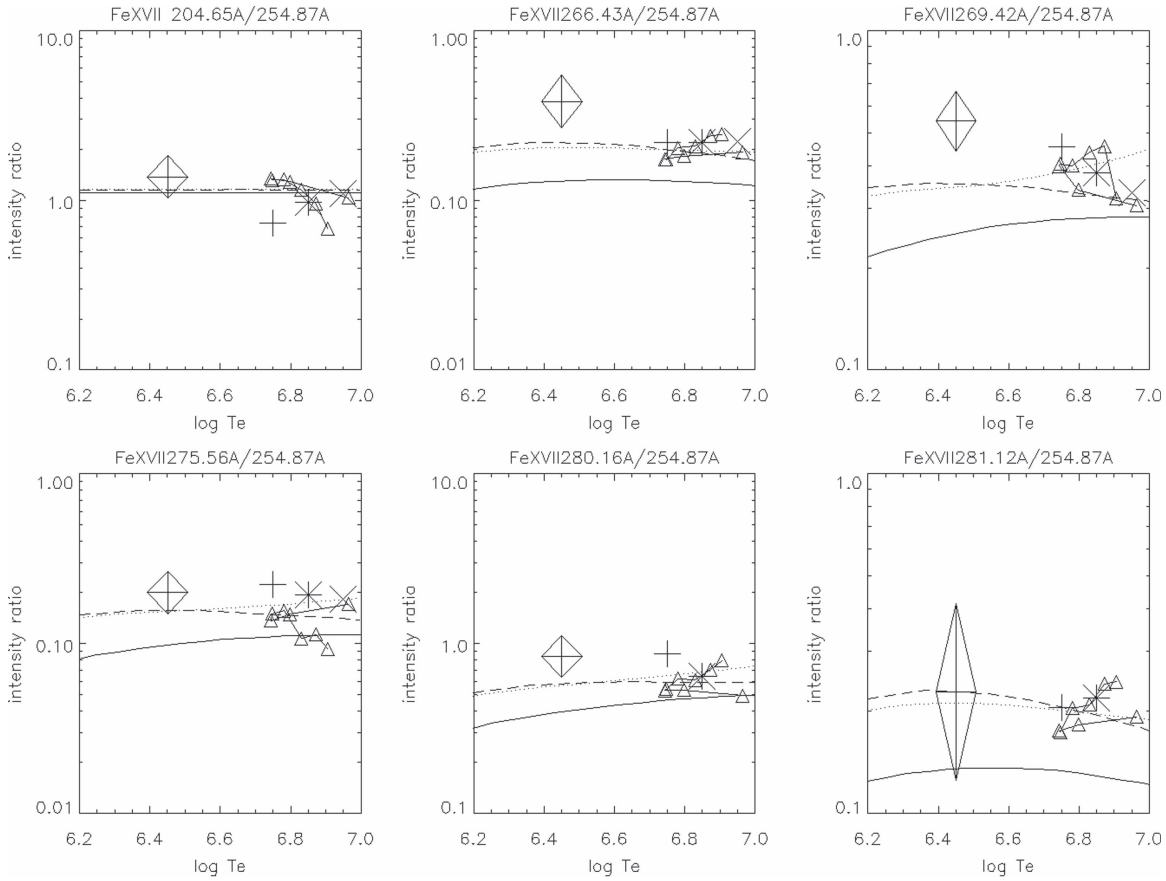

Figure 6. Fe XVII line ratios against the Fe XVII λ 254.8 line: triangles indicate the line ratios obtained from the LHD measurements, diamonds are for the ratios from the core part of the active region showing the root mean square error range, pluses are adopted from Warren et al. (2008), crosses from Doschek et al. (1991), and asterisks are from the flare data in the EIS full CCD spectral range (Del Zanna 2013) by assuming T_e of flaring plasmas; log $T_e \sim$ 6.75, 6.95, and 6.85, respectively. Corrected sensitivity calibrations are adopted from Del Zanna (2013). The solid lines indicate our model predictions, while dotted lines are from CHIANTI version 8 (Del Zanna et al. 2015) and broken lines from ADAS (Summers 2004), both with the "lgy09" data set. See also the text.

(Summers 2004) calculations, both with the "lgy09" atomic data set (Liang & Badnell 2010), show better agreement with the experiments and the observations than ours. The reason could be that the electron-impact excitation rate coefficient is calculated with the R-matrix method, which includes the resonance effect and is better than the distorted wave method in the lower collision-energy region, and more excited levels are considered.

In conclusion, pursuing accurate atomic parameters for neon-like ions of iron, one of the most abundant element in the Sun, is indispensable for our understanding of the plasma physics that takes place in the solar outer atomosphere, especially in active regions, as this ion species is created in the hottest part of steadily heated solar corona, and it provides precise diagnostic information of active regions and their circumjacent areas. Its atomic parameters are also measured in the laboratories, and they can be cross-validated with the help of theoretical models. In addition, an improvement of the radiometric calibration is expected for the EUV spectrographs that work in laboratory measurements and in solar observations.

We acknowledge the LHD experimental group for their assistance. This work is partially supported by the NIFS Collaborative Research Programs (NIFS10KLPF008 and NIFS12KLPF027). *Hinode* is a Japanese mission developed and launched by ISAS/JAXA, collaborating with NAOJ as a domestic partner, NASA and STFC (UK) as international partners. Scientific operation of the *Hinode* mission is conducted by the *Hinode* science team organized at ISAS/JAXA. This team mainly consists of scientists from institutions in the partner countries. Support for the post-launch operation is provided by JAXA and NAOJ (Japan), STFC (U.K.), NASA, ESA, and NSC (Norway).

References

Bar-Shalom, A., Klapisch, M., & Oreg, J. 2001, JQSRT, 71, 179
Brown, C. M., Feldman, U., Seely, J. F., Korendyke, C. M., & Hara, H. 2008, ApJS, 176, 511
Chowdhuri, M. B., Morita, S., Goto, M., et al. 2007, RScI, 78, 023501
Culhane, J. L., Harra, L. K., James, A. M., et al. 2007, SoPh, 243, 19
Del Zanna, G. 2008, A&A, 481, L69
Del Zanna, G. 2013, A&A, 555, A47
Del Zanna, G., Dere, K. P., Young, P. R., Landi, E., & Mason, H. E. 2015, A&A, 582, A56
Del Zanna, G., & Ishikawa, Y. 2009, A&A, 508, 1517
Dere, K. P., Landi, E., Mason, H. E., et al. 1997, A&AS, 125, 149
Dere, K. P., Landi, E., Young, P. R., et al. 2009, A&A, 498, 915
Dong, C. F., Morita, S., Goto, M., et al. 2011, RScI, 82, 113102
Doschek, G. A., Fuldman, U., & Bhatia, A. K. 1991, PhRvA, 43, 2565
Huang, X. L., Morita, S., Oishi, T., et al. 2014a, RScI, 85, 11E818
Huang, X. L., Wang, E. H., Dong, C. F., et al. 2014b, JKPS, 65, 1265
Lang, J., Kent, B. J., Paustian, W., et al. 2006, ApOpt, 45, 8689
Liang, G. Y., & Badnell, N. R. 2010, A&A, 518, A64

Murakami, I., Sakaue, H. A., Yamamoto, N., et al. 2010, PFR, 5, S2021
Murakami, I., Watanabe, T., Suzuki, C., et al. 2014, PFR, 9, 1401056
Patsourakos, S., & Klimchuk, J. A. 2006, ApJ, 647, 1452
Sakaue, H. A., Yamamoto, N., Morita, S., et al. 2011, JAP, 109, 073304
Skobelev, I., Murakami, I., & Kato, T. 2010, A&A, 511, A60
Sudo, S., & Tamura, N. 2012, RScI, 83, 023503
Sudo, S., Tamura, N., Kholopenkov, K., et al. 2002, PPCF, 44, 129
Summers, H. P. 2004, The ADAS User Manual, version 2.6, http://www.adas.ac.uk
Warren, H. P., Feldman, U., & Brown, C. M. 2008, ApJ, 685, 1277
Warren, H. P., Ugarte-Urra, I., & Landi, E. 2014, ApJS, 213, 11
Watanabe, T., Hara, H., Culhane, J. L., et al. 2007, PASJ, 59, S669
Watanabe, T., Hara, H., Yamamoto, N., et al. 2009, ApJ, 692, 1294
Watanabe, T., Hara, H., Yamamoto, N., et al. 2013, PFR, 8, 2501105
Yamamoto, N., Kato, T., Funaba, H., et al. 2008, ApJ, 689, 646
Young, P. R., Watanabe, T., Hara, H., & ariska, J. T. 2009, A&A, 495, 587
Zhang, H. M., Morita, S., & Oishi, T. 2015, JaJAP, 54, 086101